VELOCITY DISTRIBUTIONS AND MEANDER FORMATION OF RIVER CHANNELS

J. N. Kaguchwa, J. K. Kwanza and P. W. Gathia
Egerton University, Njoro, Kenya
E-mail: kaguchwajn@gmail.com

Abstract
Despite substantial research on various aspects of velocity distributions in curved meander rivers, no systematic effort has yet been made to establish the relationship between the dominant meander wavelength, discharge and the velocity distributions. In this research the secondary current theory is used in investigating the wavelength of a meander when it just emerges in a river channel. Rate of meander growth and downstream migration velocity is also investigated. To achieve this, a small-perturbation stability analysis is developed for investigation of the role of the secondary current accompanying channel curvature in the initiation and early development of meanders in open channels. Equations of the transverse velocity profile are analyzed. Since the magnitude of the vertical velocity is negligible compared to the transverse velocity in secondary currents, this study concentrates on the transverse velocity which is the radial component of the secondary current. This formulation leads to a linear differential equation which is solved for its orthogonal components which give the rates of meander growth and downstream migration. It is found that the amplitude of the meanders tends to increase and that the meanders migrate downstream. The obtained dominant discharge is important to engineers in predicting stable slope upstream of grade control-control structures and forecasting flooding in river channels. Engineers also use dominant discharge in predicting channel migration and hence they are able to evaluate and determine bridge and other highway facility locations and sizes and ascertain the need for countermeasures considering the potential impacts of channel meander migration over the life of a bridge or highway river crossing. The mathematical description meander formation will be essential to geomorphologists since it contributes to theory development and provides solutions of practical problems associated with stream channelization.

Key words: Secondary flow, transverse and longitudinal velocity, dominant wavelength and discharge, rate of meander growth, meander migration velocity (celerity)

Nomenclature

b	Channel half –width
C_r	Correction factor
F	Froude number
f	Darch-Weisbach friction factor
H	Average water depth
H_W	Depth-width ratio
k	Wave number
L	Meander wavelength
n	Manning's roughness coefficient
Q	Discharge
Q_d	Dominant discharge
Q_l	Lateral discharge
R	Hydraulic radius,
$\overline{u}$	Depth-averaged longitudinal velocity
u_*	Shear velocity at the bottom
V_G	Rate of local displacement of the centroid of the elemental Control volume of length ds .
x	Coordinate distance along the unperturbed channel axis
λ	Positive dimensionless constant
α	Von Karman constant

1 Introduction

The meandering of the rivers has been a central concern in geology and civil engineering for many years, not only because channel migration has practical implication on the land, sediment budget and navigation, but also because explanation and prediction of meandering process has remained elusive. Allan (2009) argued that when flow enters a channel bed, a helical secondary current is set up that increases flow velocity and channel depth along the outer bank in proportion to bed curvature, which encourages bank erosion. The secondary current has an intrinsic downstream scale related to flow velocity and depth; this results in gradual increase in bend amplitude and propagation of the meandering pattern upstream and downstream. Alexander (2012) noted that flow through a bend involves balancing gravitational and frictional forces by additional centrifugal force. This force increases the water-surface elevation at the outer bank and decreases it near the inner bank thereby maintaining the pressure difference that drives the flow laterally. High-momentum water in the near surface region moves from the central region of the flow toward the outer bank where it descends downward. Low-momentum water in the near bed region moves from the outer bank toward the inner bank and upward. Peter and John (1984) used secondary current theory to prove that dominant meander wavelength is directly proportional to the square root of hydraulic radius, channel width and inversely proportional to channel roughness. Anderson (1967) emphasized on the importance of channel width, depth and Froude number in determining the dominant wavelength.

Braudrick *et al.,* (2009) argued that experimental meander migration is faster as compared to most natural channels. Channel migration that involves alluvial river meander and planform deformation is a major consideration in designing bridge crossings and other transportation facilities in affected areas. It causes the channel alignment and approach conditions present during construction to deteriorate as the downstream channel location changes.

Ferro and Porto (2012) noted that identification of the value of dominant or bankfull discharge has been a subject of great challenge to scientists and engineers during the last decades. This is because the value is largely adopted for stream-management decisions like predicting stable slope upstream of grade-control structures, designing moderate to large sized hydraulic structures and forecasting flooding in a river channel. Mozaffari *et al.,* (2011) noted that the presence of strong secondary currents and their interaction with the topography of the channel bed in river bends have significant effects on the distributions of longitudinal and transverse velocity and consequently the shear stress across the width and length of a bend. However there is no mathematical model that has utilized secondary current theory to relate channel topography (e.g. meander wavelength and meander amplitude) with velocity distributions (e.g. depth-averaged velocity, longitudinal surface velocity and bed shear velocity). A mathematical model relating dominant wavelength with dominant discharge and velocity distribution has also not been obtained. Therefore the main purpose of this investigation is to address the above two issues.

2 Analytical Model

A channel with a finite value of the radius of curvature is considered. The radius of curvature assumes an infinite value where the channel is straight. The analysis of flow in curved channels as presented herein is restricted to subcritical flow with hydrostatic pressure distribution and the channel depth is assumed to be much less than the width and the radius of curvature. This is mostly observed at the lower course of a river channel. In deriving the equation of motion, a differential element of fluid in polar coordinate system is used as shown in Fgure 1.

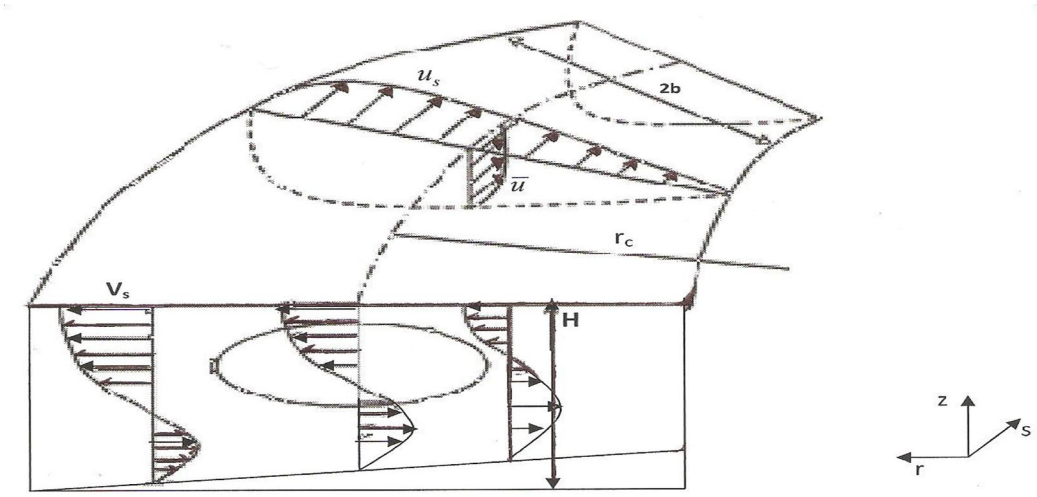

Figure 1: Transverse velocity profile in curved channel

Won and Young (2010) used force-momentum equations in polar cylindrical coordinates to relate the longitudinal velocity (u), transverse velocity (v), vertical velocity (w), the longitudinal slope (S), transverse water surface slope (S_r), transverse shear stress (τ_r), Longitudinal shear stress (τ_S) and radius of curvature (r) as follows:

$$\frac{\partial u}{\partial t}+u\frac{\partial u}{\partial s}+v\frac{\partial u}{\partial r}+w\frac{\partial u}{\partial z}=-\frac{uv}{r}+gS+\frac{\partial \tau_s}{\rho \partial z} \quad \text{.....(1)}$$

$$\frac{\partial v}{\partial t}+u\frac{\partial v}{\partial s}+v\frac{\partial v}{\partial r}+w\frac{\partial v}{\partial z}=\frac{u^2}{r}-gS_r+\frac{\partial \tau_r}{\rho \partial z} \quad \text{.....(2)}$$

For steady flow, the time derivatives $\frac{\partial u}{\partial t}$ and $\frac{\partial v}{\partial t}$ in equations (1) and (2) can be dropped. Also second order terms $w\frac{\partial v}{\partial z}$, $w\frac{\partial u}{\partial z}$, $v\frac{\partial v}{\partial r}$, and $\frac{uv}{r}$ can be eliminated because v and w are small compared with u. Substituting all these in equation (2), yields;

$$u\frac{\partial v}{\partial s}=\frac{u^2}{r}-gS_r+\frac{\partial \tau_r}{\rho \partial z} \quad \text{.....(3)}$$

Equation (3) represents fluid motion in the transverse direction. The mechanism of secondary flow development can be described by each term of Eq. (3). The left-hand side in Eq. (3) is longitudinal variation of transverse velocity. In the right-hand side, the first term represents centrifugal acceleration, the second term represents the transverse water-surface slope and the third term represents the turbulent shear. From equation (3) the transverse water surface velocity (v_s), longitudinal water surface velocity (u_s) and radius of curvature from centerline of the channel (r_c) are related as;

$$u_s\frac{\partial v_s}{\partial s}=\frac{{u_s}^2}{r_c}-gS_r+\left.\frac{\partial \tau_r}{\rho \partial z}\right|_{z=H} \quad \text{.....(4)}$$

Baek *et al.,* (2006) noted that;

$$\left.\frac{\partial \tau_r}{\rho \partial z}\right|_{z=H}=-\frac{2\alpha u_*}{H}v_s \quad \text{.....(5)}$$

$$s_r = \frac{\bar{u}^2}{g r_c} \quad \text{.....(6)}$$

Substituting (5) and (6) into (4), yields;

$$\frac{\partial v_s}{\partial s} + \frac{2\alpha u_*}{H u_s} v_s = \frac{\bar{u}}{r_c}\left[\frac{u_s}{\bar{u}} - \frac{\bar{u}}{u_s}\right] \quad \text{.....(7)}$$

Henderson (1966) observed that;

$$\frac{u_s}{\bar{u}} = \frac{m+1}{m} \quad \text{..... (8)}$$

Where m is the friction term in steady flow which is defined as;

$$m = \frac{\alpha R^{1/6}}{n\sqrt{g}} \quad \text{..... (9)}$$

Substituting equation (8) into (7) and since v_s is a function of s only, it yields;

$$\frac{dv_s}{ds} + \left[\frac{2m\alpha u_*}{H\bar{u}(m+1)}\right] v_s = \frac{1}{r_c}\left[\frac{\bar{u}(2m+1)}{m(m+1)}\right] \quad \text{.....(10)}$$

Since meander initiate in a river channel at a very large value of radius of curvature (*r*), the transverse slope according to equation (6) is almost negligible and therefore the channel cross-section can be assumed to be rectangular when meander just forms in a river channel. The channel-alignment perturbation will be taken to be a migrating sinusoid as shown in the Figure 3.

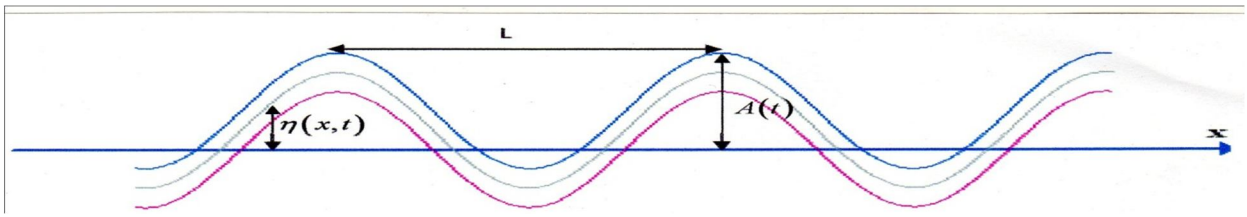

Figure 3: Sinusoidal Perturbation

According to Peter and John (1984), the perturbation displacement from the convex bank to concave bank is given by;

$$\eta(x,t) = A(t)\sin k(x - ct) \quad \text{.....(11)}$$

$$k = \frac{2\pi}{L} \quad \text{.....(12)}$$

Peter and John (1984) observed that;

$$\frac{1}{r_c} = -\frac{d^2\eta}{dx^2} \quad \text{.....(13)}$$

Substituting (11) into (13) yields;

$$\frac{1}{r_c} = k^2 A \sin k(x - ct) \quad \text{.....(14)}$$

Substituting (14) into (10) yields;

$$\frac{dv_s}{dx} + \left[\frac{2m \propto u_*}{H\bar{u}(m+1)}\right] v_s = \frac{k^2 A\bar{u}(2m+1)}{m(m+1)} \sin k(x - ct) \quad \text{.....(15)}$$

Equation (15) is linear ordinary differential equation. The solution of this equation that is periodic and independent of the initial condition is:

$$v_s = \frac{k^2 H\bar{u}^2 A(2+\frac{1}{m})}{\left[4m^2 \propto^2 u_*^2 + k^2 H^2 \bar{u}^2 (m+1)^2\right]^{\frac{1}{2}}} \sin k\left(x - ct - \frac{\gamma}{k}\right) \quad \text{.....(16)}$$

Where $\tan\gamma = \frac{H\bar{u}(m+1)k}{2m \propto u_*}$ .....(17)

The phase shift (γ) must vary between zero and pie because the primary flow is assumed to be stronger than the secondary current. The velocity of secondary current attains maximum when the phase shift is approximately equal to 0.5π . This happens when the inertial term is dominant over the friction term. The velocity of secondary current is in phase with the channel axis displacement when the phase shift is approximately equal to zero. Peter and John (1984), argued that as the control volume moves laterally in a curved river channel, the difference between the rates of these processes at the concave and convex banks is given by;

$$\frac{dQ_l}{ds} = V_G \quad \text{.....(18)}$$

Since the channel centerline is curved, the centroid of the central volume is not at mid width of the channel, but is displaced toward the concave bank, the displacement being inversely proportional to the radius of the curvature. Peter and John (1984) argued that for a rectangular channel cross-section, the displacement is $b/3r_c$. They obtained the rate of lateral migration as;

$$V_G = \frac{\partial\eta}{\partial t} - \frac{b^2}{3}\frac{\partial^3\eta}{\partial t \partial x^2} \quad \text{.....(19)}$$

They also argued that the rate of differential erosion-deposition across the channel is proportional to the rate of a fictious lateral transport of sediment from the outer to the inner bank. Therefore;

$$\frac{dQ_l}{ds} = \lambda V_s \quad \text{.....(20)}$$

Substitution of (20) into (18) yields;

$$V_G = \lambda v_s \quad \text{.....(21)}$$

Substitution of (21) into (19) yields;

$$\frac{\partial\eta}{\partial t} - \frac{b^2}{3}\frac{\partial^3\eta}{\partial t \partial x^2} = \lambda v_s \quad \text{.....(22)}$$

Substitution of (11) and (16) into (22) and simplifying yields:

$$\frac{1}{A}\frac{dA}{dt} = kc\cot k(x-ct) + \frac{\lambda k^2 H\bar{u}^2\left(2+\frac{1}{m}\right)\sin k\left(x - ct - \frac{\gamma}{k}\right)}{\left(1+\frac{b^2k^2}{3}\right)\left[4m^2 \propto^2 u_*^2 + k^2 H^2 \bar{u}^2 (m+1)^2\right]^{\frac{1}{2}} \sin k(x-ct)} \quad \text{.....(23)}$$

Integrating equation (23) and simplifying it yields;

$$\ln A = C_1 - \left[1 - \frac{\lambda kH\bar{u}^2\left(2+\frac{1}{m}\right)\sin\gamma}{\left(1+\frac{b^2k^2}{3}\right)\left[4m^2 \propto^2 u_*^2 + k^2 H^2 \bar{u}^2 (m+1)^2\right]^{\frac{1}{2}} C}\right] \ln\sin k(x-ct) + \frac{\lambda k^2 H\bar{u}^2\left(2+\frac{1}{m}\right)(\cos\gamma)t}{\left(1+\frac{b^2k^2}{3}\right)\left[4m^2 \propto^2 u_*^2 + k^2 H^2 \bar{u}^2 (m+1)^2\right]^{\frac{1}{2}}} \quad \text{.....(24)}$$

Equation (24) is satisfied if;

$$C = \frac{\lambda k H \bar{u}^2 \left(2 + \frac{1}{m}\right) \sin\gamma}{\left(1 + \frac{b^2 k^2}{3}\right)\left[4m^2 \propto^2 u_*^2 + k^2 H^2 \bar{u}^2 (m+1)^2\right]^{\frac{1}{2}}} \quad \text{.....(25)}$$

Therefore equation (24) reduces to;

$$\ln A = C_1 + \frac{\lambda k^2 H \bar{u}^2 \left(2 + \frac{1}{m}\right)(\cos\gamma) t}{\left(1 + \frac{b^2 k^2}{3}\right)\left[4m^2 \propto^2 u_*^2 + k^2 H^2 \bar{u}^2 (m+1)^2\right]^{\frac{1}{2}}} \quad \text{.....(26)}$$

Since at $t = 0,\ A = A_0$, equation (26) simplifies;

$$A = A_0 \exp\left(\frac{2\lambda \propto (2m+1) u_*}{H(m+1)^2}\right)\left(\frac{\sin^2\gamma}{1+\beta^2 \tan^2\gamma}\right) t \quad \text{.....(27)}$$

Where $\beta^2 = \frac{4m^2 \propto^2 u_*^2 b^2}{3H^2 \bar{u}^2 (m+1)^2}$ and $\sin^2\gamma = \frac{H^2 \bar{u}^2 (m+1)^2}{4m^2 \propto^2 u_*^2 k^{-2} + H^2 \bar{u}^2 (m+1)^2}$

Equation (27) therefore simplifies to;

$$A = A_0 \exp\left(8\lambda \propto^3 m^2 t (2m+1) u_*^3 H \bar{u}^2\right)\left[\frac{1}{\left(\frac{4m^2 \propto^2 u_*^2}{k^2} + \beta^2 H^2 \bar{u}^2 (m+1)^2\right)\left(4m^2 \propto^2 u_*^2 + k^2 H^2 \bar{u}^2 (m+1)^2\right)}\right] \quad \text{.....(28)}$$

The exponent in equation (28) is positive for all *k*. Therefore the amplitude of the sinusoidal perturbation increases exponentially with time.

It is observed in equation (28) that the exponent tends to zero again for *k*=∞. However there is a dominant wave number for which the rate of growth is maximum. The dominant wave number for which the rate of growth is maximum is observed when $\frac{\partial^2 A}{\partial t \partial k} = 0$. Substituting this in (28) and simplifying yields.

$$\tan\gamma = \beta^{-\frac{1}{2}} \qquad \text{Where } 0 < \gamma \leq \pi/2 \quad \text{.....(29)}$$

Substitution of (17), into (29) yields;

$$k = \left[\frac{\sqrt{12} m \propto u_*}{H \bar{u} (m+1) b}\right]^{\frac{1}{2}} \quad \text{.....(30)}$$

Equation (30) defines the dominant wave number. Substitution of (12) into (30) yields;

$$L = \pi \left[\frac{2bH\bar{u}(m+1)}{m \propto u_* \sqrt{3}}\right]^{\frac{1}{2}} \quad \text{.....(31)}$$

Substitution of (10) into (31) yields;

$$L = \pi \left[\frac{BHu_s}{\sqrt{3} \propto u_*}\right]^{\frac{1}{2}} \quad \text{.....(32)}$$

where $B = 2b$. Since $Q = BH\bar{u}$ equation (32) simplifies to;

$$L = \pi \left[\frac{Q u_s}{\propto u_* \bar{u} \sqrt{3}}\right]^{\frac{1}{2}} \quad \text{.....(33)}$$

Therefore the predicted/dominant meander wavelength as a function of dominant discharge is given by equation (33). Substitution of (30) into (17) and then (8) yields;

$$\tan\gamma = \left(\frac{\sqrt{3}H_w}{\propto}\frac{u_s}{u_*}\right)^{\frac{1}{2}} \quad \text{.....(34)}$$

Making γ the subject in (34) yields;

$$\gamma = \tan^{-1}\left(\frac{\sqrt{3}H_w}{\propto}\frac{u_s}{u_*}\right)^{\frac{1}{2}} \qquad \text{where, } 0 \le \gamma < \pi/2 \quad \text{.....(35)}$$

Substitution of (30), into (25) and after some algebraic manipulations yields;

$$C = \frac{\lambda\bar{u}(2m+1)\sin^4\gamma}{m(m+1)} \quad \text{.....(36)}$$

According to Won and Young (2010), $m = \alpha\bar{u}(u_*)^{-1}$ while Francisco (2010) noted that $u_* = 0.354\bar{u}\sqrt{f}$ and therefore $m = 1.131f^{-0.5}$. Substituting all this in equation (36) yields.

$$C = \frac{\lambda\bar{u}(0.884\sqrt{f}+2)\sin^4\gamma}{0.884f^{-0.5}+1} \quad \text{.....(37)}$$

Equation (37) defines the migration velocity of the meander pattern which is also called the celerity (C). Substitution of (30) into (28) and after some algebraic manipulations, equation of the amplitude of the dominant wave is obtained as follows;

$$A = A_0\exp\frac{6\lambda H\bar{u}^2(2m+1)(\cos^4\gamma)t}{m^2B^2 \propto u_*} \quad \text{.....(38)}$$

Since $m = 1.131f^{-0.5}$ equation (38) simplifies to;

$$A = A_0\exp\left[37.529\lambda H\bar{u}B^{-2}\alpha^{-1}\cos^4\gamma\left(\sqrt{f}+2.262\right)t\right] \quad \text{.....(39)}$$

2 Results and Discussion

The foregoing analysis demonstrates that secondary currents produced by small periodic perturbations in the alignment of an otherwise straight channel can cause the amplitude of the perturbations to increase with time, and produce downstream migration of the resulting meanders. The stability analysis is linear and it's therefore applicable only to small-amplitude meanders. It's observed from equation (32) that the predicted/dominant wavelength (*L*) at which meandering occurs is proportional to square root of the ratio of longitudinal surface velocity to bed shear velocity. This is the ratio at which meandering occurs and it therefore reduces as meandering process continues. This ratio can only be maximized if the shear velocity is minimized and longitudinal surface velocity is maximized. It is observed from equation (37) and (39) that channel roughness increases as meandering process continues. This is in agreement with the existing theory since more alternate bars and ripples which causes an increase in roughness forms as meandering process occurs. Hence there is a need to determine the ratio of longitudinal surface velocity to shear velocity at which meandering occurs.

Several laboratory experiments have been conducted to determine the dominant wavelength (L). Based on equation (32) the flume experimental results obtained by Anderson *et al.,* (1975) were used to determine the above ratio. This was done by rearranging equation (32) to get;

$$\frac{u_*}{u_s} = \frac{\pi^2 BH}{\alpha L^2\sqrt{3}} \quad \text{.....(40)}$$

Anderson *et al.,* (1975) presented a data from 167 laboratory flume experiments which were carried out by nine groups of researchers. To determine the ratio $\frac{u_*}{u_s}$ the results from the same flume type (*S-E*) were used to avoid errors that might arise by using results from different flume types. The mean value was found to be 0.01. Hence $U_r = \frac{u_s}{u_*} = 100$.

Substituting the above mean in equation (32) and taking $\alpha = 0.4$ (Helmut, 2012) yields;

$L_{KE} = 37.74\sqrt{BH}$ .....(41)

Equation (41) gives the approximate predicted/dominant meander wavelength $\left(L_{KE}\right)$ obtained from experimental flume data.

Due to errors that occur in any experiment, simulations were carried out using **MATLAB** version 7.9 to determine again the ratio of $\frac{u_s}{u_*} = U_r$ at which meander forms in a river channel. Using equation (32), Figures 3a and 3b were obtained for different values of channel breadth (B) and depth (H)

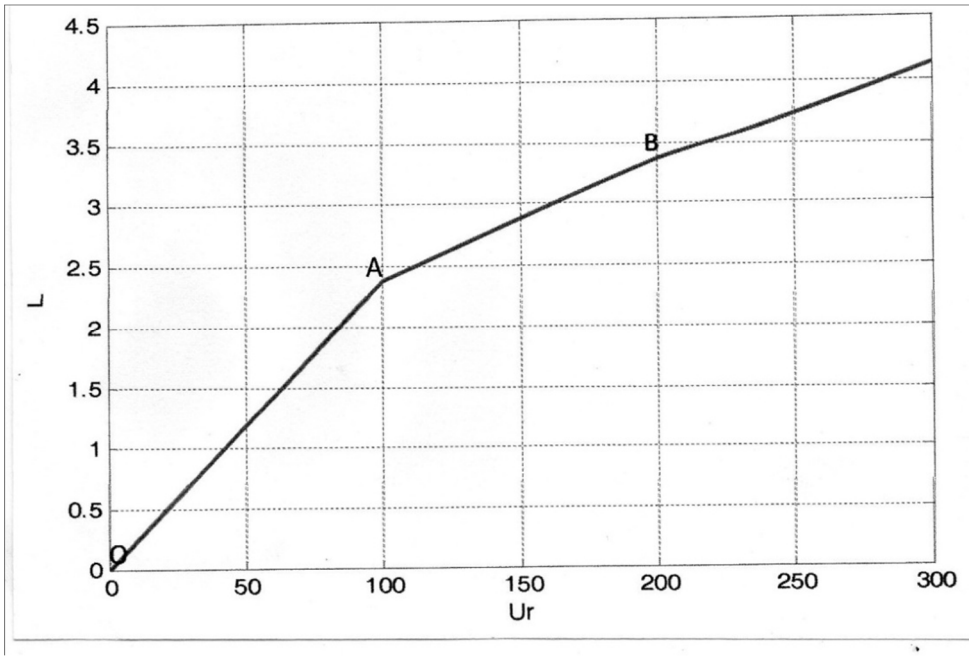

Figure 3a: Predicted Wavelength (L) against the Ratio of Longitudinal Surface Velocity to Shear Velocity; B=0.4917 and H=0.00809

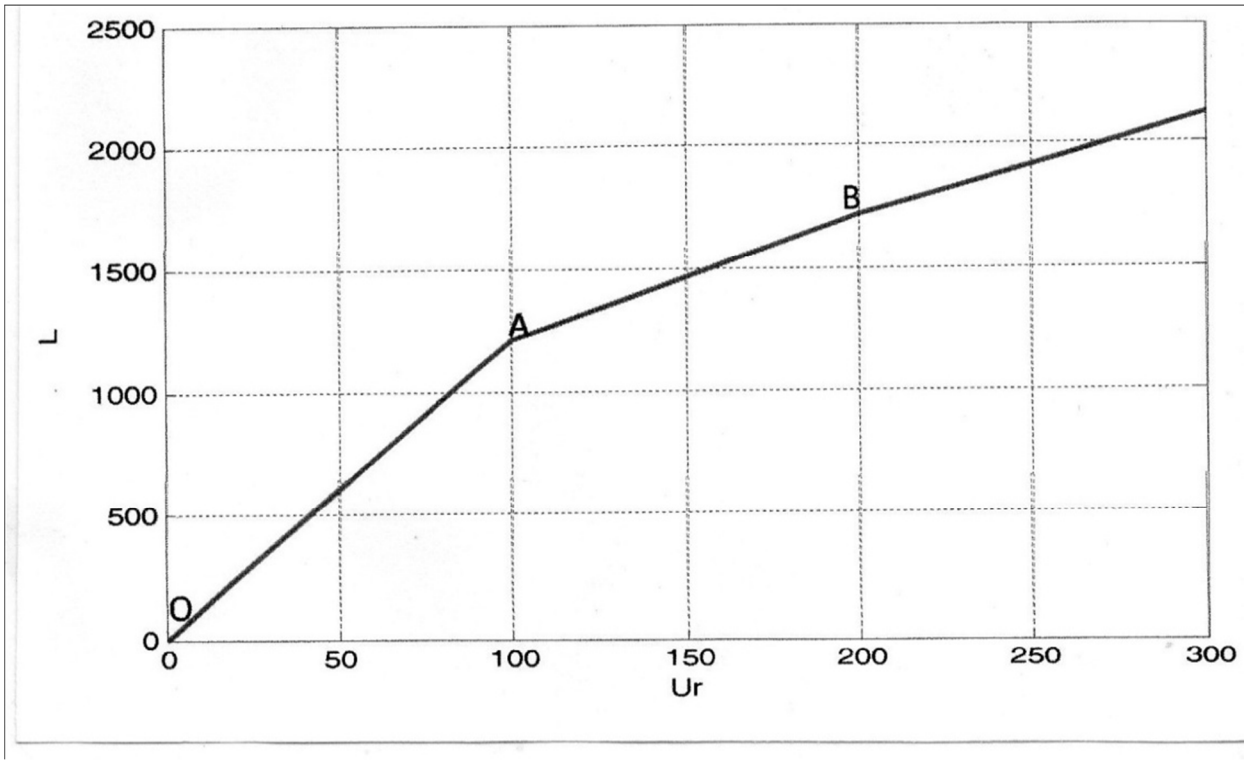

Figure 3b: Predicted Wavelength (L) against the Ratio of Longitudinal Surface Velocity to Shear Velocity; B=127.1 and H=8.2.

It's observed from Figures 3a and 3b that the channel remains straight beyond point *B*. From *B* to *A,* meandering takes place. From *A* to *O,* braiding is observed. Meandering therefore forms in a river channel at a maximum value of U_r being *200* and the minimum value being *100*. The average value of U_r at which meandering forms is therefore *150*. Therefore river channel will remain straight when $U_r > 200$, transition from straight to meandering occurs when $150 < U_r \leq 200$, meandering occurs when $U_r = 150$ transition from meandering to braiding occurs when $100 < U_r < 150$ and braiding occurs when $U_r \leq 100$. Therefore as U_r decreases, the channel pattern changes from straight to meandering and then from meandering to braiding. This is because of the fact that U_r can only reduce when u_* increases and according to Francisco (2010) the friction factor will also increase. An increase in friction factor causes more resistance to the flow and hence deposition which leads to formation bars that forms braiding.

Substitution of the average value of U_r (150) into equation (32) yields;

$$L_{KS_A} = 46.23\sqrt{BH} \quad \text{.....(42)}$$

Substitution of the maximum value of U_r (200) into equation (32) yields;

$$L_{KS_M} = 53.38\sqrt{BH} \quad \text{.....(43)}$$

There is need to determine the best model from the three obtained above for the purpose of predicting the meander wavelength small amplitude (laboratory experiments) meanders. The models will also be compared with what has been obtained by other researchers.

For small amplitude meanders, models as obtained in equation (41), (42) and (43) were tested using the Anderson *et al.,* (1975) experimental results given in table 2. This is summarized in *table 1* below. The results are also compared with what was obtained by Hansen (1967), Anderson (1967) and Peter and John (1984). All results are compared with the observed meander wavelength (L_m)**.** To determine the most accurate model that can predict the meander wavelength for small amplitude meanders, Figures 4and 5 are drawn using the results in Table 1.

Table 1: Comparison of the Predicted and the Measured Experimental Wavelength

Run Number	M-1-2	M-1-3	M-1-5	117	118	119	126
Width (cm) (B)	107	136	123	44.35	42.75	49.17	41.70
Depth (cm) (H)	1.50	1.77	1.75	.773	.789	.809	.957
Froude No. (F)	.227	.280	.314	.741	.852	.803	.572
Pattern	M	M	M	M	M	M	M
Resistance(Chezy)	0.0974	0.0569	0.0481	0.0147	0.0102	0.0110	0.0182
Sediment discharge	-	-	-	1.40	2.50	1.44	0.57
Observed Wave Length (L_m)	4.91	4.59	6.07	2.8	3.0	3.0	3.9
$L_H = 56Hf^{-1}$	1.03	2.09	2.45	3.54	5.19	4.94	3.54
$L_{A2} = 2\sqrt{\pi HBC^{-1}}$	1.44	2.31	2.37	1.72	2.04	2.13	1.66
$L_A = 72\sqrt{HBF}$	4.34	5.91	5.92	3.63	3.89	4.10	3.42
$L_{PJ} = 20\sqrt{0.5RBf^{-1}}$	1.99	3.19	3.28	2.37	2.81	2.94	2.30
$L_{KE} = 37.74\sqrt{BH}$	4.78	5.86	5.54	2.21	2.20	2.38	2.38
$L_{KS_A} = 46.23\sqrt{BH}$	5.86	7.17	6.78	2.71	2.68	2.92	2.92
$L_{KS_M} = 53.38\sqrt{BH}$	6.76	8.28	7.83	3.12	3.10	3.37	3.37

L_H -Predicted wavelength by Hansen (1967). L_A and L_{A2} -Predicted wavelength by Anderson (1967). L_{PJ} -Predicted wavelength by Peter and John (1984). L_{KE} , L_{KS_A} and L_{KS_M} - Predicted wavelength by Kaguchwa, Kwanza and Gathia.

To determine the most accurate model that can predict the meander wavelength for small amplitude meanders, origin software was used in drawing *figures 4* and *5* using the results in Table 1.

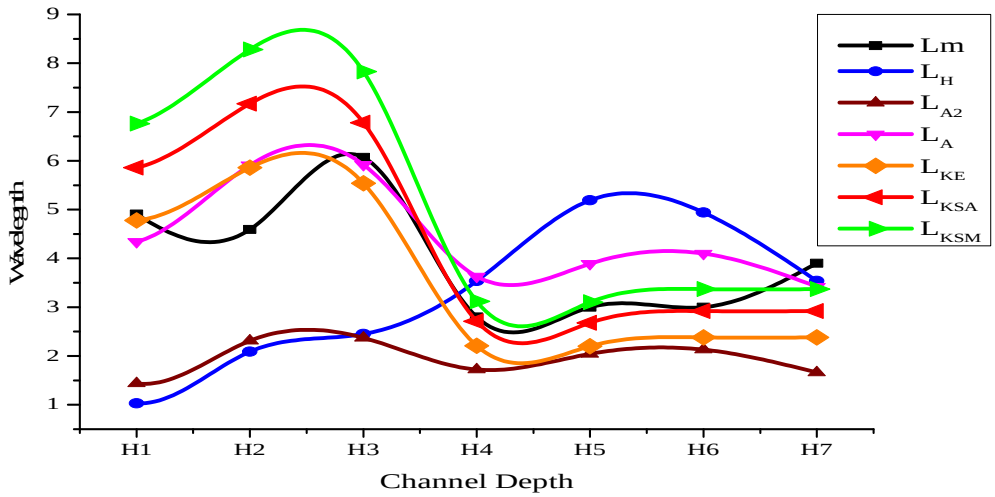

Figure 4: Dominant wavelength against depth for small amplitude meanders

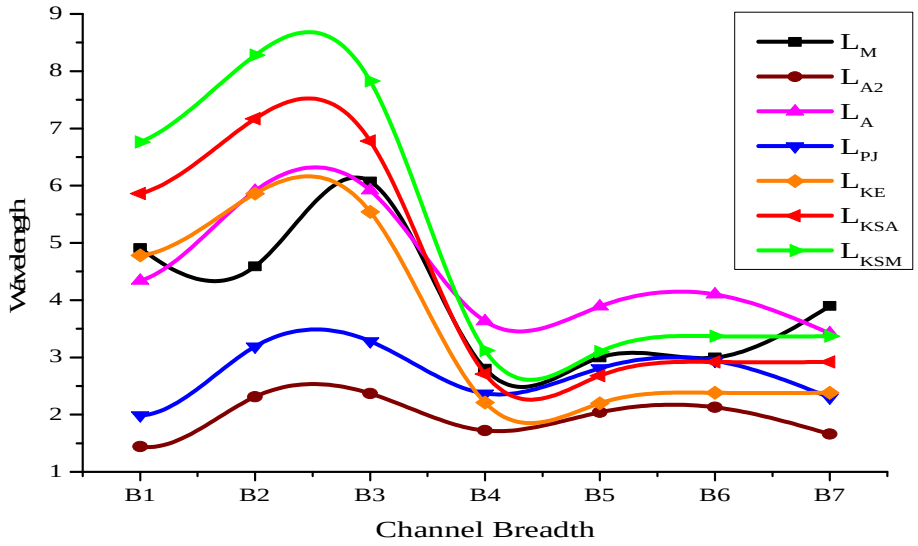

Figure 5: Dominant wavelength against breadth for small amplitude meanders

It's observed from *figure 4 and 5* that $L_{KS_A} = 46.23\sqrt{BH}$ is the best model in estimating the dominant wavelength for small amplitude meanders and more so the laboratory experiments. However, a large deviation of the predicted wavelength (L_{KS_A}) and the measured wavelength (L_m) is observed in *H1, H2* and *H7* in *figure 4* and also in *B1, B2* and *B7* in *figure 5*. The deviation in H7 and B7 is due to a sharp decrease in sediment discharge. The same could have caused the deviation in *H1, H2, B1* and *B7*. Leopold *et al.*, (1964), Solari *et al.*, (2002) and Fagherazzi *et al.*, (2004) noted that at smaller scale, channel meander bends are formed as a result of sediment transport processes.

Substituting $\frac{u_s}{u_*} = 150$ in equation (33) yields;

$$L_{KS_A} = 46.23\sqrt{\frac{Q_d}{\bar{u}}} \quad \text{.....(44)}$$

After evaluating the dominant wavelength, the dominant discharge can be evaluated using equation (44) for a given value of the average velocity.

To obtain detailed information on how different flow parameters relate with one in determining whether meander growth dominates meander migration and vice versa, the ratio of meander growth rate $\left(dA/dt\right)$ to meander migration velocity (C) is calculated.

Differentiating (38) with respect to *t* and dividing with (36) yields;

$$\frac{1}{C}\frac{dA}{dt} = \frac{2\alpha u_* A}{H u_s} \quad \text{.....(45)}$$

It's observed from equation (45) that the ratio increases with decrease in depth and vice versa. Therefore shallow channels will exhibit a strong tendency to grow than to migrate. Very deep channels will exhibit a strong tendency to migrate than to grow. Very rough channels will exhibit a strong tendency to grow than to migrate while smooth channels will exhibit a strong tendency to migrate than to grow.

4 Conclusions

Analytical Models were developed to investigate the role of secondary flow in the initiation and early development of river meandering. The model $L_{KS_A} = 46.23\sqrt{BH}$ is the best in estimating the dominant meander wavelength. Any discharge exceeding the calculated dominant discharge will automatically cause flooding. The obtained dominant wavelength, discharge, rate of meander growth and celerity models obtained in this research should be seriously considered by the engineers when constructing roads and bridges in a region of an unstable channel. The amplitude of a small sinusoidal perturbation in the alignment of an initially straight channel tends to increase exponentially with time. Analytical expressions were also developed for the rate of amplitude growth and the velocity of meander migration. Shallow channels were found to exhibit a strong tendency to grow than to migrate. Very deep channels will exhibit a strong tendency to migrate than to grow. Very rough channels will exhibit a strong tendency to grow than to migrate while smooth channels will exhibit a strong tendency to migrate than to grow. Although the models were generated for a small-perturbation analysis, they are found to be in good agreement with measured wavelengths of meandering river channels. The results of the analytical model are also in agreement with experimental data on meandering streams. It's therefore noted that secondary currents play a major role in the initiation and development of meanders. The theory developed has provided a hydrodynamic explanation of meandering process.

Appendices
Experiments from Multi-Purpose Channel and Tilting Flume Experiment

Table 2: Experimental Results obtained from multi-purpose channel and tilting flume

Run Number	M-1-2	M-1-3	M-1-5	117	118	119	126
Width (cm) (B)	107	136	123	44.35	42.75	49.17	41.70
Depth (cm) (H)	1.50	1.77	1.75	.773	.789	.809	.957
Froude No. (F)	.227	.280	.314	.741	.852	.803	.572
Resistance (Chezy)	0.0974	0.0569	0.0481	0.0147	0.0102	0.0110	0.0182
Sediment discharge	-	-	-	1.40	2.50	1.44	0.57
Observed Wave Length (Lm)	4.91	4.59	6.07	2.8	3.0	3.0	3.9

Source: Anderson *et al.,* (1975)

References

Alexander, N.S., (2012). Structure of Turbulent Flow in a Meander Bend of a Lowland River. *Journal of water resources research*, **48**: doi: 10.1029/2011WR10765.

Allan, D.H., (2009). How to Make a Meander River. *National academy of sciences*, **106**: pp 16936-16941.

Anderson, A. G., (1967). *On the Development of Stream Meanders*. Proc. 12th Congress IAHR, Fort Collins, Colorado, **1**: pp 370-378.

Anderson, A. G., Parker, G., and Wood, A., (1975). *The Flow and Stability Characteristics of Alluvial River Channels*. Project report no 161, University of Minnesota-U.S.A.

Baek, K.O., Seo I.O. and Lee, K. W., (2006). New Equation on Streamwise Variation of Secondary Flow in Meandering Channels. *Journal of Civil Eng.,* **26,** 4B: pp 371-378.

Braudrick C. A., William E. D., Glen T. L. and Leonard S. S. (2009). Experimental Evidence for the Conditions Necessary to Sustain Meandering in Coarse-bedded Rivers. *National academy of sciences*, **40**: pp16936-16941.

Fagherazzi, S., Gabet, E. J. and Furbish, D. J., (2004). The Effect of Bidirectional Flow in Tidal Channel Planforms. *Journal of Earth Surface Processes and Landforms*, **29**: pp 295-309.

Ferro, V. and Porto, P., (2012). Identifying a Dominant Discharge for Natural Rivers in Southern Italy. *Geomorphology*, **139**: pp 313-321.

Francisco J.M., (2010). *Flow Resistance in Open Channels with Fixed and Movable Bed*. Federal Intragency Conference- June 27-2010.

Hansen, E., (1967). The Formation of Meanders as a Stability Problem. Basic Res. Prog. Rep. 13, Hydraul. Lab., Tech. Univ. Denmark, Lyngby.

Helmut Z. B., (2012). Universal Equations and Constants of Turbulent Motion. *Journal of Physica Scripta, ar* Xiv: 1203.5042Vl.

Henderson, F. M., (1966). *Open channel flow*. Mackmillan Publishing Co.

Mozaffari, J., Amiri, T.E. and Blanckaert, K., (2011). Experimental Investigations to Determine the Distribution of Longitudinal Velocity in River Bends. *Research journal of environmental sciences*, **5**: pp 544-556.

Leopold, L. B., Wolman, M. G. and Miller J. P., (1964). Fluvial Processes in Geomorphology. Dover Publications Inc, New York.

Won, S. and Young J. J., (2010). Velocity Distribution of Secondary Currents in Curved channels. 9th International Conference on Hydrodynamics. October 11-15, 2010 Shanghai, China.